



Research paper

# Fluorescence spectroscopy of vibronic polaritons of molecular aggregates in optical microcavities



Zhedong Zhang\*, Shaul Mukamel

Department of Chemistry, University of California Irvine, Irvine, CA 92697, USA

## ARTICLE INFO

## Article history:

Received 22 December 2016

In final form 7 February 2017

Available online 10 February 2017

## ABSTRACT

We compute the fluorescence spectrum of a molecular aggregate with electronic and vibrational degrees of freedom, described by Holstein model, in an optical cavity. The redistribution of oscillator strength among the vibronic polaritons due to strong interaction with the cavity mode and its effect on superradiance is investigated. Simulations demonstrate the scaling of spectra with the coupling strength to cavity and with aggregate size.

© 2017 Elsevier B.V. All rights reserved.

## 1. Introduction

Microcavities provide a tool for manipulating the interaction strength between matter and photons. Atoms strongly coupled to cavity modes can be described by the hybrid matter/photon states, known as polaritons. The underlying theoretical framework, cavity quantum electrodynamics (Cavity-QED), has been well developed [1–3] and realized in numerous experiments for atoms [4]. Strong coupling in cavity-QED has been recently demonstrated for organic molecules [5–8]. Polaritons have been recently investigated in chromophore aggregates [9–11]. Purely vibrational polaritons have been recently demonstrated in molecular aggregates by using Infrared and Raman spectroscopies [9,10,12,13]. Vibronic polaritons involving coupled excitons and vibrations have been studied using the Holstein Hamiltonian [14,15].

Recent studies have shown the potential of cavity photons to enhance cooperative signals, such as superradiance and subradiance [16,17], in atomic and ionic ensembles [18–20], stemming from the strong collective interaction of many molecules with the vacuum mode of cavity. The vibronic coupling owing to the electronic relaxation has been shown to significantly influence the exciton dynamics [21–25], especially in the vicinity of avoided crossing [11,26–28]. The interaction with cavity modes can give rise to the strong correlation between molecules, which results in the interesting competition between photonic and vibronic contributions to the excitonic dynamics. The decoupling of collective electronic states due to vibronic coupling was predicted [14,15]. However, superradiance may be limited by nuclear vibrations, which will be explored further in this article.

In this work, we investigate the effect of vibrational modes on the cooperativity of molecules in a microcavity, by means of the fluorescence spectrum. Previous studies have shown the elimination of vibronic coupling to excitons for the lowest-energy vibronic polariton (LVP) [14]. We will study the effect of cooperativity for highest-energy vibronic polariton (HVP) and examine its variation with aggregate size. A deviation from  $N^2$ -scaling of the fluorescence intensity will be demonstrated where  $N$  is the amount of molecules in aggregate.

## 2. The Holstein model for an aggregate in a cavity

We consider a linear aggregate made of  $N$  identical molecules, each of which has a single vibrational mode. The system is described by the Holstein Hamiltonian

$$H_{ex} = \varepsilon \sum_{n=1}^N \sigma_n^+ \sigma_n^- + J \sum_{n=1}^{N-1} (\sigma_n^+ \sigma_{n+1}^- + \sigma_{n+1}^+ \sigma_n^-) + \hbar \omega_{\text{vib}} \sum_{n=1}^N b_n^\dagger b_n + \sum_{n=1}^N \lambda \hbar \omega_{\text{vib}} \sigma_n^+ \sigma_n^- (b_n + b_n^\dagger) \quad (1)$$

where  $\varepsilon$  is the electronic excitation energy of each molecule and  $J$  denotes the dipole-dipole coupling between adjacent molecules.  $\sigma_n^+$  ( $\sigma_n^-$ ) is the Pauli operator, which creates (annihilates) an exciton in the  $n$ -th molecule.  $b_n$  annihilates a vibron of the vibrational mode in the  $n$ -th molecule in aggregate. The Huang-Rhys factor  $\lambda^2$  represents the interaction strength of the excitons to vibrational modes. The aggregate is further coupled to a cavity mode in terms of

$$H_{ex-cav} = g \sum_{n=1}^N (\sigma_n^+ a + \sigma_n^- a^\dagger) \quad (2)$$

\* Corresponding author.

E-mail address: [zhedongz@uci.edu](mailto:zhedongz@uci.edu) (Z. Zhang).

in rotating-wave approximation and the total Hamiltonian then reads  $H = H_{ex} + \hbar\omega_c a^\dagger a + H_{ex-cav}$ .  $a$  is the annihilation operator of photons.  $g$  stands for the strength of molecule-photon interaction which can be tuned by adjusting the incident angle of the electromagnetic wave into the cavity. The cavity frequency  $\omega_c$  is resonant with the central frequency of single electronic excitation band ( $\omega_c \simeq \varepsilon$ ) for the optical transitions and the subsequently strong coupling to photons creates the polaritons. The number of excitations  $M = \sum_{n=1}^N \sigma_n^+ \sigma_n^- + a^\dagger a$  is conserved and  $H$  is block-diagonal with respect to  $M$ .

Therefore, it is convenient to introduce a dressed basis which takes into account the vibronic-induced renormalization of the excitation energy of single molecule. This can be achieved by the polaron transformation:  $\tilde{H} = e^S H e^{-S}$  with the generating operator  $S = \sum_{n=1}^N \lambda_n \sigma_n^+ \sigma_n^- (b_n^\dagger - b_n)$  [29]. The transformed Hamiltonian is

$$\begin{aligned} \tilde{H} = & \sum_{n=1}^N \tilde{\varepsilon}_n \sigma_n^+ \sigma_n^- \\ & + J \sum_{n=1}^{N-1} \left( \sigma_n^+ \sigma_{n+1}^- e^{i\lambda_n (b_n^\dagger - b_n) - i\lambda_{n+1} (b_{n+1}^\dagger - b_{n+1})} + \sigma_{n+1}^+ \sigma_n^- e^{-i\lambda_n (b_n^\dagger - b_n) + i\lambda_{n+1} (b_{n+1}^\dagger - b_{n+1})} \right) \\ & + \hbar\omega_{\text{vib}} \sum_{n=1}^N b_n^\dagger b_n + g \sum_{n=1}^N \left( \sigma_n^+ a e^{i\lambda_n (b_n^\dagger - b_n)} + \sigma_n^- a^\dagger e^{-i\lambda_n (b_n^\dagger - b_n)} \right) \\ & + \hbar\omega_c a^\dagger a \end{aligned} \quad (3)$$

where  $\tilde{\varepsilon}_n = \varepsilon - \lambda_n^2 \hbar\omega_{\text{vib}}$ . The energy spectrum will be obtained by diagonalizing the Hamiltonian  $\tilde{H}$  in truncated space with the ground-state and single-excitation manifolds only. The basis is  $|\varphi_i\rangle = |\{n_s^{(i)}\}, m^{(i)}\rangle \otimes |\{v_j^{(i)}\}\rangle$  and  $n_s^{(i)} = 0, 1$ ;  $s = 1, 2, \dots, N$  for the excitons in the individual molecules.  $m^{(i)}$  represents the photon occupation and  $v_j^{(i)}$ ;  $j = 1, 2, \dots, N$  denotes the vibrational occupation for the individual molecules. The ground state of the system is  $|G\rangle = |\{0_s\}, 0\rangle \otimes |\{0_j\}\rangle$  where  $s = 1, 2, \dots, N$  labels the electronic excitation of individual molecules and  $j = 1, 2, \dots, N$  labels the nuclear vibrations for each molecule correspondingly. We further assume low temperature  $\hbar\omega_{\text{vib}} \gg k_B T$ , so that only the vibrational state  $v = 0$  is occupied initially. The transformed Hamiltonian in Eq. (3) was diagonalized numerically by including only three vibrational states on each molecule.

### 3. The absorption spectrum

The linear absorption spectrum (LA) of our vibronic polariton model is [30,31]

$$S_{LA}(\omega) = \sum_e \frac{\omega_{eg} |\mu_{eg}|^2 \frac{\Gamma}{2}}{(\omega - \omega_{eg})^2 + \frac{\Gamma^2}{4}} \quad (4)$$

where the electric dipole is  $\mu = \sum_{n=1}^N \mu_n (\sigma_n^+ + \sigma_n^-)$  in which  $\mu_n$  stands for the electric dipole moment between ground and single-excited states of single molecule.  $\omega_{eg} = (E_e - E_g)/\hbar$  and  $\Gamma$  is the electronic dephasing rate. We hereafter assume  $\Gamma = 0.04$  eV hereafter. The dipole transition moment is  $\mu_{eg} = \langle e | \mu | g \rangle$  where  $|g\rangle, |e\rangle$  are the ground- and excited-states in the polariton basis obtained through the diagonalization of the Hamiltonian  $\tilde{H}$  in Eq. (3). In the simulations we assume  $\mu_n \simeq 3.7D$  which is typical for porphyrin[32,33].

Fig. 2 shows the calculated absorption for weak, intermediate and strong coupling to cavity photons (top to bottom). As shown in the top and middle panels in Fig. 2 when the interaction to photons is weak, the spectrum shows vibrational progressions. The strong coupling (bottom in Fig. 2) leads to two bright states, which show up as the two strong narrow peaks. We will denote them as

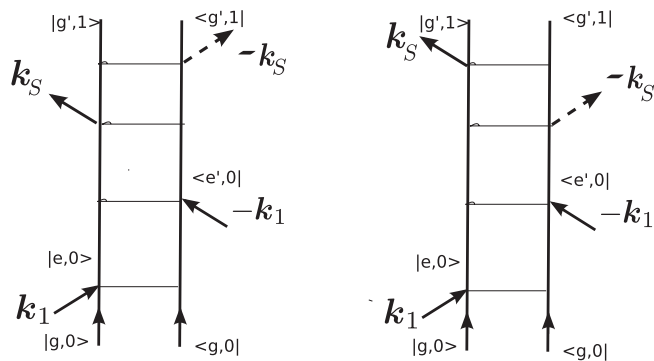


Fig. 1. Diagrams for the fluorescence signal. 0 denotes the vacuum and 1 is the single photon state of field.

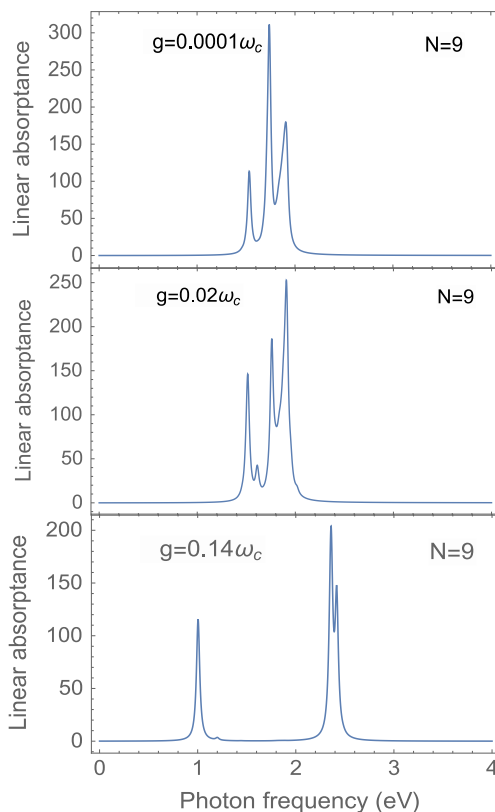


Fig. 2. The absorption spectrum of a vibronic aggregate ( $N = 9$ ) with strong coupling to nuclear vibrations. The Huang-Rhys factor is  $\lambda = 0.9$ . (Top panel) Weak interaction with cavity:  $g = 0.0001\hbar\omega_c$ ,  $\lambda = 0.9$ . (Middle panel) Intermediate interaction with cavity:  $g = 0.02\hbar\omega_c$ ,  $\lambda = 0.9$ . (Bottom panel) Strong interaction with cavity:  $g = 0.14\hbar\omega_c$ ,  $\lambda = 0.9$ . Other parameters are  $\varepsilon = 1.65$  eV,  $J = 0.07$  eV,  $\hbar\omega_{\text{vib}} = 0.17$  eV and  $\omega_c = 1.64$  eV.

the highest-energy vibronic polariton (HVP) and lowest-energy vibronic polariton (LVP). This is consistent with the Dicke model [16] which predicted the superradiance due to strong coupling with photons.

### 4. The fluorescence spectrum

The fluorescence signal is obtained by recording the spontaneous light emission at frequency  $\omega_s$ , following the excitation by an  $\omega_L$  photon. This is depicted in the Feynman diagrams in Fig. 1 and the fluorescence signal is given by [34]

$$S_{FL}(\omega_L, \omega_s) = \frac{4\pi\omega_s}{Vh^3} \sum_{e, g_{prime}} \sum_{g_{prime}} \frac{\mu_{eg} \mu_{g'prime} \mu_{eg'prime} \mu_{g'prime}}{\omega_{g'prime}^2 + \gamma^2} \times \left\{ \frac{\gamma((\omega_L - \omega_{eg})(\omega_s - \omega_{g'prime}) + \Gamma^2) - \Gamma\omega_{g'prime}(\omega_s - \omega_L + \omega_{eg} - \omega_{g'prime})}{\Gamma^2((\omega_L - \omega_{eg})^2 + (\omega_s - \omega_{g'prime})^2 + \Gamma^2) + (\omega_s - \omega_{eg})^2(\omega_s - \omega_{g'prime})^2} \right. \\ \left. - \frac{\gamma((\omega_L - \omega_{eg})(\omega_s - \omega_{g'prime}) + \Gamma^2) - \Gamma\omega_{g'prime}(\omega_s - \omega_L + \omega_{eg} - \omega_{g'prime})}{\Gamma^2((\omega_L - \omega_{eg})^2 + (\omega_s - \omega_{g'prime})^2 + \Gamma^2) + (\omega_s - \omega_{eg})^2(\omega_s - \omega_{g'prime})^2} \right\} \quad (5)$$

where  $\gamma$  denote the dephasing rate of single excitations of the vibronic polaritons. We assume  $\gamma = 0.01$  eV. We will study the fluorescence signal and will further explore the vibronic effect on cooperativity, in the regime of strong coupling to cavity mode.

The simulated fluorescence signals for strong, mediated and weak coupling regimes are shown in Fig. 3 for a 5-molecule aggregate. For strong molecule-cavity interaction, only diagonal elastic peaks  $\omega_L = \omega_s$  that correspond to the two branches of single vibronic polariton are observed. When decreasing the molecule-cavity coupling strength (Figs. 3(a), (c) and (e)), inelastic scattering shows up. This can be elucidated from Fig. 3(b), (d) and (f) by the fact that the positions of two cross peaks are displaced by  $\sim 0.17$  eV  $\simeq \hbar\omega_{vib}$  and  $\sim 0.34$  eV  $\simeq 2\hbar\omega_{vib}$  with respect to the diagonal peak. The inelastic scattering is thus attributed to the vibrational transitions and reflects the breakdown of cooperativity.

### 5. Scaling of spectra with aggregate size

In order to study the vibronic effect on the cooperativity in the strong cavity coupling regime, we have simulated the variation of

fluorescence signal  $S_{FL}$  with the number  $N$  of molecules. The parameters are  $\varepsilon = 1.65$  eV,  $J = 0.07$  eV,  $\hbar\omega_{vib} = 0.17$  eV [32,33]. The cavity mode is set to be resonant with the central frequency of the single electronic excitation band,  $\hbar\omega_c \simeq 1.64$  eV and the excitons therefore strongly couple to the cavity:  $g = 0.14\hbar\omega_c \gg \varepsilon - \hbar\omega_c$ . In Fig. 4 we show the effect of vibrations on the cooperativity by calculating the intensity of the elastic signal  $S_{FL}$  according to Eq. (5) at  $\omega_s = \omega_L$  for different aggregate sizes.  $\omega_L$  is tuned to the excitation energies of LVP or HVP. As shown in Fig. 4 for strong ( $\lambda = 0.9$ , top left) and weak vibronic couplings ( $\lambda = 0.001$ , top right), the lowest-energy polariton in the single-excitation manifold scales as: (top left)  $S_{FL}(\omega_L, \omega_s = \omega_L) = 0.532N + 0.378N^2$ , (top right)  $S_{FL}(\omega_L, \omega_s = \omega_L) = 0.656N + 0.411N^2$  and we find that the  $N^2$ -term dominates as the aggregate size increases. This further indicates that the spontaneous emission of LVP is superradiant and the cooperativity is then protected by the cavity. This is consistent with earlier finding where the vibronic coupling was shown to be suppressed by cavity [14]. However, as shown in the bottom panels in Fig. 4 the cooperativity in HVP is broken by the vibronic coupling and the signal no longer shows an  $N^2$ -scaling. The breakdown of cooperativity in HVP is further elucidated in Fig. 5, by the weak cross peak (at  $\omega_s \simeq 2.01$  eV) beside the diagonal one (at  $\omega_s \simeq 2.36$  eV) that denotes the elastic scattering, although the diagonal peaks still dominate the 2D spectrum. The red and blue curves in the right panel in Fig. 5 show slices of the signal  $S_{FL}$  in the 2D plot, with  $\omega_L = 1.05$  eV (red) and  $\omega_L = 2.36$  eV (blue) respectively. The low cross peak shown by the blue line in Fig. 5 (right) indicates the inelastic scattering and is contributed by tran-

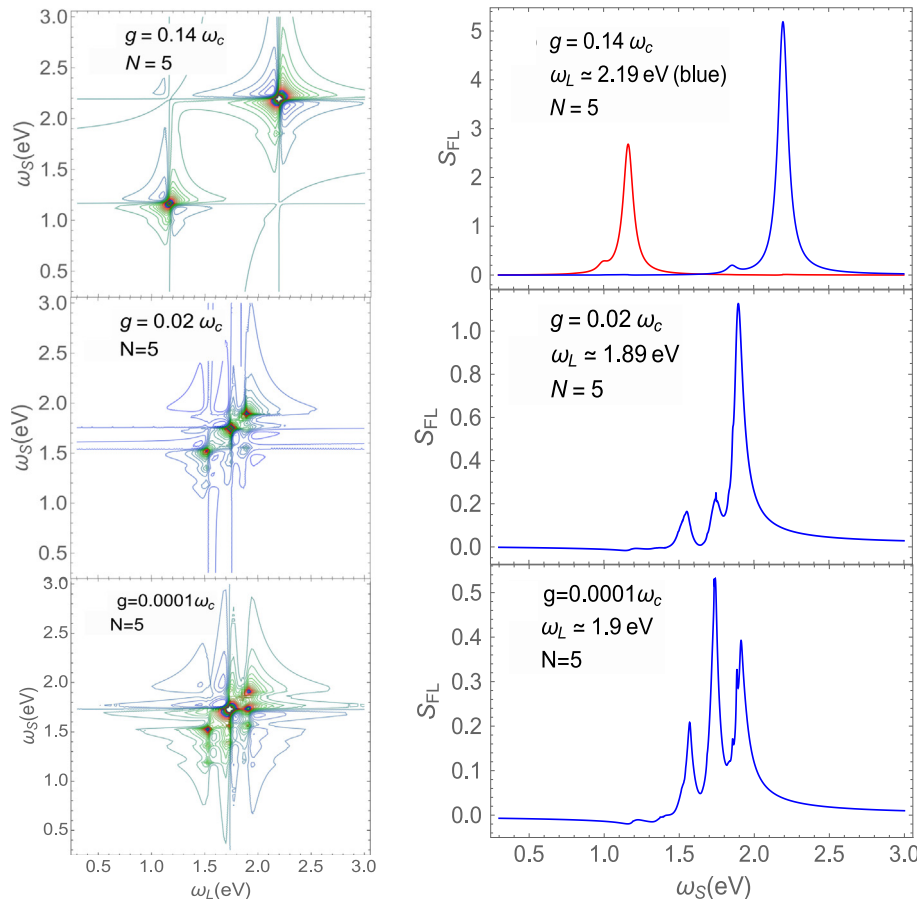


**Fig. 3.** (Left column) 2D fluorescence spectrum (FL) based on Eq. (5) and (right column) 1D slides for a fixed pulse frequency  $\omega_L$ . (Top panel):  $g = 0.14\hbar\omega_c$  (strong coupling);  $\omega_L \simeq 1.16$  eV and  $\omega_L \simeq 2.19$  eV are for red and blue lines, respectively. (Middle panel):  $g = 0.02\hbar\omega_c$  (intermediate coupling) and  $\omega_L \simeq 1.89$  eV. (Bottom panel):  $g = 0.0001\hbar\omega_c$  (weak coupling) and  $\omega_L \simeq 1.9$  eV. Other parameters are  $\varepsilon = 1.65$  eV,  $J = 0.07$  eV,  $\hbar\omega_{vib} = 0.17$  eV and  $\hbar\omega_c = 1.64$  eV. (For interpretation of the references to color in this figure legend, the reader is referred to the web version of this article.)

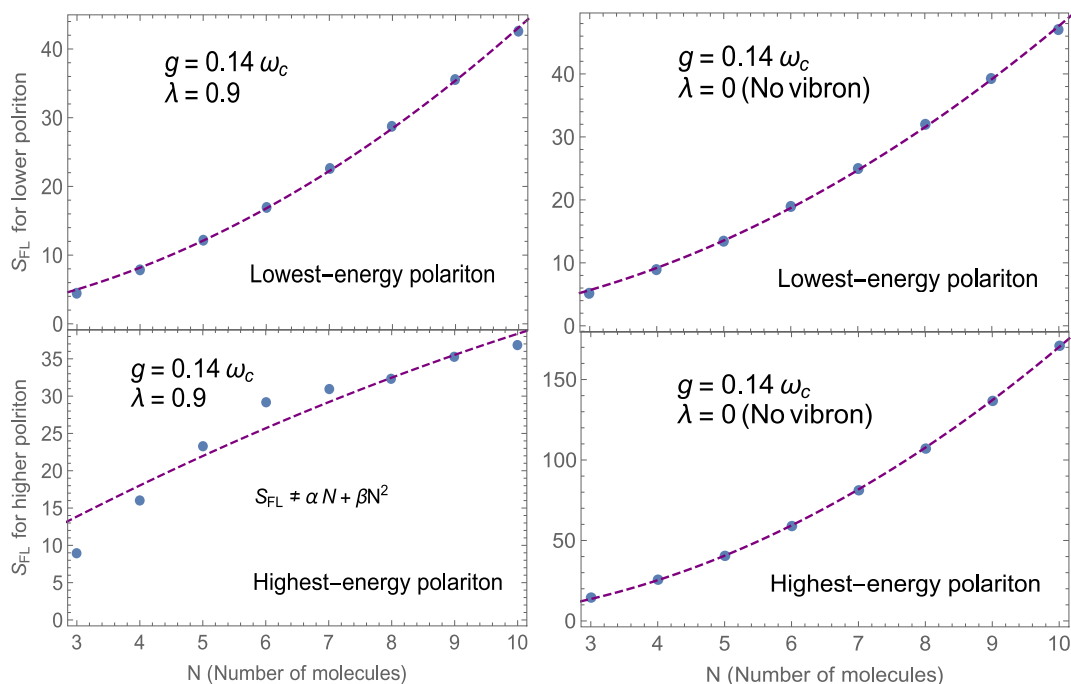


**Fig. 4.** Elastic fluorescence intensity as a function of  $N$ . The lower and higher polaritons correspond to LVP and HVP, according to the linear absorption in the bottom panel in Fig. 2. Blue spots represent the data for different  $N$  and the dashed purple lines are from data-fitting. Top row are the fluorescence intensity of lowest-energy polariton while bottom row are for highest-energy polariton; left column and right column correspond to the case  $\lambda = 0.9$  (strong polariton-vibron coupling) and the case without vibron, respectively. The fitting equations of signal intensity with  $N$  are (top left)  $S_{FL} = 0.532N + 0.378N^2$ , (top right)  $S_{FL} = 0.656N + 0.411N^2$  and (bottom right)  $S_{FL} = -0.803N + 1.782N^2$ . (Bottom left) The signal intensity does not scale as  $\alpha N + \beta N^2$ . Parameters are  $\varepsilon = 1.65$  eV,  $J = 0.07$  eV,  $\hbar\omega_{vib} = 0.17$  eV and  $\hbar\omega_c = 1.64$  eV.

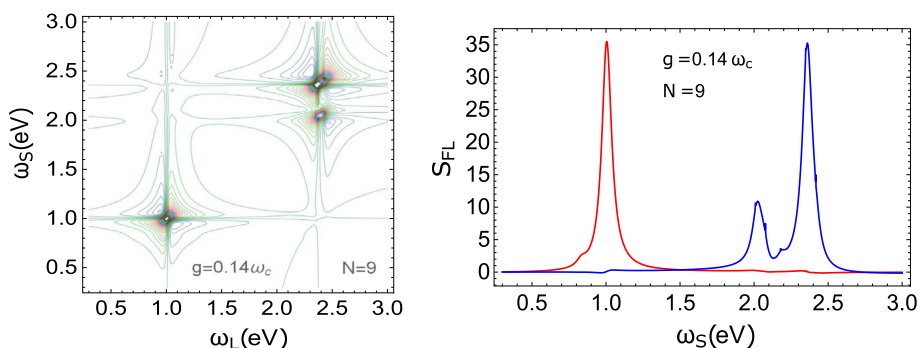


**Fig. 5.** (Left) Fluorescence spectra as a function of pump and signal frequencies  $\omega_L$ ,  $\omega_S$  given in Eq. (5), for a 9-molecule aggregate. (Right) Blue: pulse frequency is set to be 2.36 eV which is resonant with the highest-energy polariton. Red: pulse frequency is set to be 1.05 eV which is resonant with the lowest-energy polariton. Other parameters are the same as that in Fig. 2. (For interpretation of the references to color in this figure legend, the reader is referred to the web version of this article.)

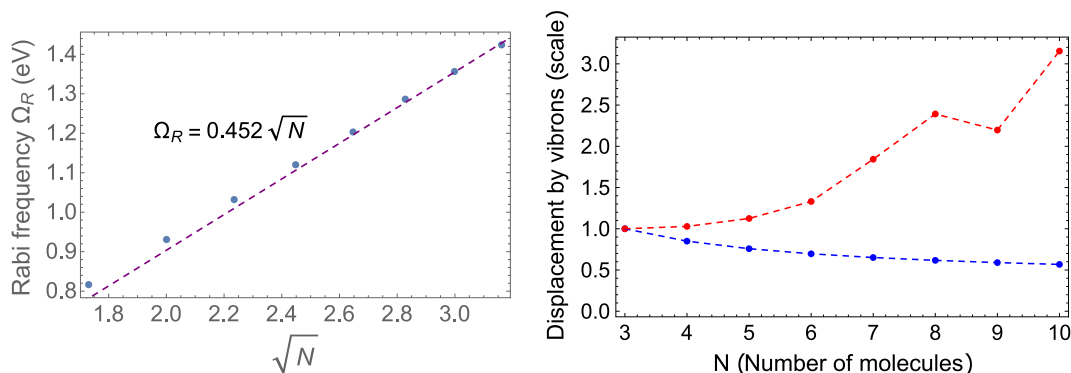


**Fig. 6.** (Left) Rabi frequency between the two branches of vibronic polaritons (LVP and HVP) with respect to aggregate size where dashed line is from data-fitting. (Right) Deviation of the minimum of excited-state energy surfaces from ground state. Red and blue lines are for HVP and LVP, respectively.  $g = 0.14\hbar\omega_c$  (strong coupling to cavity) and Huang-Rhys factor is  $\lambda = 0.9$ . The parameters are the same as that in Fig. 2. (For interpretation of the references to color in this figure legend, the reader is referred to the web version of this article.)

sition between different vibrational states because of  $\sim 0.335 \text{ eV} \approx 2\hbar\omega_{\text{vib}}$  displacement of the position of the diagonal peak at  $\omega_s \approx 2.36 \text{ eV}$ .

It is also interesting to look at the Rabi splitting between LVP and HVP, which was evaluated from the absorption spectra with different aggregate size. The  $\sqrt{N}$ -scaling seems to be maintained in the strongly vibronic coupling regime, as shown in Fig. 6 (left). This implies the limit of linear absorption on exploring the effect of nuclear vibrations, although it was popularly applied on studying many aspects [13,35,36].

In order to explore the mechanism of the diminished cooperativity for HVP compared to LVP, we examine the reorganization of nuclear configurations for HVP and LVP, since this affects the Huang–Rhys factor for polaritons. To quantify this effect, the deviation of the nuclear configuration that minimizes the excited energy from that of ground state should be evaluated in terms of  $\sum_s \alpha_s (b_s + b_s^\dagger)$ . In such spirit, we have

$$D = \langle \Psi_M | \sum_{s=1}^N \lambda_s \sigma_s^+ \sigma_s^- (b_s + b_s^\dagger) | \Psi_M \rangle$$

$$= \sum_{ij=1}^{D_1} \sum_{s=1}^N U_{M,i}^{(1),T} U_{j,M}^{(1)} \lambda_s n_s^{(i)} \prod_{p=1}^N \delta_{n_p^{(i)}, n_p^{(j)}} \delta_{m^{(i)}, m^{(j)}} \prod_{\substack{r=1 \\ (r \neq s)}}^N \delta_{v_r^{(i)}, v_r^{(j)}} \left( \sqrt{v_s^{(i)}} \delta_{v_s^{(i)}, v_s^{(j)}-1} \right. \\ \left. + \sqrt{v_s^{(i)} + 1} \delta_{v_s^{(i)}, v_s^{(j)}+1} \right) - 2 \sum_{i=1}^{D_1} \sum_{s=1}^N U_{M,i}^{(1),T} U_{i,M}^{(1)} \lambda_s^2 n_s^{(i)} \quad (6)$$

where  $M = \text{HVP, LVP}$  and  $|\Psi_M\rangle$  refers to the corresponding eigenstate.  $U^{(1)}$  represents the orthogonal matrix diagonalizing the Hamiltonian Eq. (3) in single-excitation manifold.  $n_s^{(i)} = \langle \varphi_i | \sigma_s^+ \sigma_s^- | \varphi_i \rangle$  where  $|\varphi_i\rangle \equiv |\{n_s^{(i)}\}, m^{(i)}\rangle \otimes |\{v_r^{(i)}\}\rangle$  is the  $i$ -th basis state in single-excitation manifold. Fig. 6(right) illustrates the reorganization of nuclear configurations of HVP and LVP, in response to the amount of molecules. For large  $N$ , the deviation of the minimum of the energy surface of HVP from ground state is much larger than that of LVP. The increase of  $D$  with  $N$  further implies the strong electronic dephasing due to nuclear motion, for HVP. In contrast, for LVP,  $D$  decreases with the amount of molecules, which indicates the reduction and weak electronic dephasing caused by nuclear motion. Moreover, Fig. 6 (right) elucidates that the reorganization of nuclear configuration of HVP is much stronger as well as much more sensitive than that of LVP, in response to the size of the aggregate in cavity. Thus LVP shows a robust but weak reorganization of nuclear configuration while the HVP does not. Therefore the analysis above provides the explanation of why the suppression of superradiance can be observed only for HVP.

## 6. Conclusions

By computing the fluorescence signals we demonstrate the suppression of cooperativity of a molecular in a cavity by vibronic coupling. The superradiance is eroded for the highest-energy polariton, but not for the lowest-energy one. This is shown by the breakdown of  $N^2$ -scaling of fluorescence intensity, although the Rabi splitting between the highest-energy and lowest-energy polaritons can still scale as  $\sqrt{N}$ . This implies that the fluorescence signal is more informative than the absorption spectra. This suppression of cooperativity originates from the reorganization of the nuclear configurations. In contrast, this reorganization

becomes robust but weak for the lowest-energy polariton. The robustness of the breakdown of cooperativity in our conclusion can be verified by the simulations under different parameter regimes, of which the details are omitted here to avoid redundancy.

We have considered a single aggregate in the cavity. The cooperativity between different aggregates is of further interest and the properties of many aggregates in cavity has been recently studied [37,38].

## Acknowledgement

We gratefully acknowledge the support from the grant NSF-CHE-1361516.

## References

- [1] E.M. Purcell, Phys. Rev. 69 (1946) 674.
- [2] E.T. Jaynes, F.W. Cummings, Proc. IEEE 51 (1963) 89.
- [3] S. Haroche, Rev. Mod. Phys. 85 (2013) 1083.
- [4] S. Nuszmann, K. Murr, M. Hijlkema, B. Weber, A. Kuhn, G. Rempe, Nat. Phys. 1 (2005) 122.
- [5] S. Kena-Cohen, S.R. Forrest, Nat. Photon. 4 (2010) 371.
- [6] J. Bellessa, C. Symonds, J. Laverdant, J.M. Benoit, J.C. Plenet, S. Vignoli, Electronics 3 (2014) 303.
- [7] A. Cacciola, O. Di Stefano, R. Stassi, R. Saija, S. Savasta, ACS Nano 8 (2014) 11483.
- [8] Y. Tsuchimoto, H. Nagai, M. Amano, K. Bando, H. Kondo, Appl. Phys. Lett. 104 (23) (2014) 4.
- [9] P. Saurabh, S. Mukamel, J. Chem. Phys. 144 (2016) 124115.
- [10] A. Shalabney, J. George, J. Hutchison, G. Pupillo, C. Genet, T.W. Ebbesen, Nat. Commun. 6 (2015) 5981.
- [11] M. Kowalewski, K. Bennett, S. Mukamel, J. Phys. Chem. Lett. 7 (2016) 2050.
- [12] A. Shalabney, J. George, H. Hiura, J.A. Hutchison, C. Genet, P. Hellwig, T.W. Ebbesen, Angew. Chem. Int. Ed. 54 (2015) 7971.
- [13] J. del Pino, J. Feist, F.J. Garcia-Vidal, New J. Phys. 17 (2015) 053040.
- [14] F.C. Spano, J. Chem. Phys. 142 (2015) 184707.
- [15] F. Herrera, F.C. Spano, Phys. Rev. Lett. 116 (2016) 238301.
- [16] R.H. Dicke, Phys. Rev. 93 (1954) 99.
- [17] M. Gross, S. Haroche, Phys. Rep. 93 (1982) 301.
- [18] R. DeVoe, R. Brewer, Phys. Rev. Lett. 76 (1996) 2049.
- [19] M.O. Scully, Phys. Rev. Lett. 102 (2009) 143601.
- [20] M.O. Scully, A.A. Svidzinsky, Science 325 (2009) 1510.
- [21] N. Christensson, H.F. Kauffmann, T. Pullerits, T. Mancal, J. Phys. Chem. B 116 (2012) 7449.
- [22] Z.D. Zhang, J. Wang, J. Phys. Chem. B 119 (2015) 4662.
- [23] E.J. O'Reilly, A. Olaya-Castro, Nat. Commun. 5 (2014) 3012.
- [24] J.M. Womick, A.M. Moran, J. Phys. Chem. B 115 (2011) 1347.
- [25] Z.D. Zhang, J. Wang, Sci. Rep. 6 (2016) 37629.
- [26] M. Kowalewski, K. Bennett, J.R. Rouxel, S. Mukamel, Phys. Rev. Lett. 117 (2016) 043201.
- [27] M. Kowalewski, K. Bennett, S. Mukamel, J. Chem. Phys. 144 (2016) 054309.
- [28] J. Galego, F.J. Garcia-Vidal, J. Feist, Phys. Rev. X 5 (2015) 041022.
- [29] O. Madelung, Introduction to Solid-State Theory, 3rd ed., Springer-Verlag, 1996 (Translated by B.C. Taylor).
- [30] D. Abramavicius, B. Palmieri, D.V. Voronine, F. Sanda, S. Mukamel, Chem. Rev. 109 (2009) 2350.
- [31] A.L. Fetter, J.D. Walecka, Quantum Theory of Many-particle Systems, Dover Publications, New York, 2003.
- [32] F.V.A. Camargo, H.L. Anderson, S.R. Meech, I.A. Heisler, J. Phys. Chem. B 119 (2015) 14660–14667.
- [33] R. Giovannetti, The use of spectrophotometry UV–Vis for the study of porphyrins, in: J. Uddin (Ed.), Macro To Nano Spectroscopy, InTech, 2012, <http://dx.doi.org/10.5772/38797>, Available from: <<http://www.intechopen.com/books/macro-to-nano-spectroscopy/the-use-of-spectrophotometry-uv-vis-for-the-study-of-porphyrins>>.
- [34] S. Mukamel, Nonlinear Optical Spectroscopy, Oxford University Press, 1995.
- [35] Y. Zhang, J.D. Biggs, S. Mukamel, Chem. Phys. Chem. 16 (2015) 2006.
- [36] M. Newcomb, J.A. Halgrimson, J.H. Horner, E.C. Wasinger, L.X. Chen, S.G. Sligar, Proc. Natl. Acad. Sci. USA 105 (2008) 8179.
- [37] D.M. Coles et al., Nat. Mater. 13 (7) (2014) 712.
- [38] D.G. Lidzey, D.D.C. Bradley, A. Armitage, S. Walker, M.S. Skolnick, Science 288 (2000) 1620.